LCC – 0040 06/06/00
Fermilab-FN-690

Linear Collider Collaboration Tech Notes

Estimates of Dispersive Effects in a Bent NLC Mail Linac

25 May 2000

Leo Michelotti and Michael Syphers

Fermi National Accelerator Laboratory
Batavia, IL

Abstract: Each arm of the NLC Main Linac is almost 11 km in length; including the final focus region, the total complex extends over 30 km. Were it to be constructed using straight-line tunneling, its sagitta relative to a gravitational equipotential surface would be about 18 meters. While that seems like a small number, its impact on pumping requirements is significant. Further, if the tunnel is dug using ``cut-and-fill'' methods, the increased cost of moving the extra dirt must also be taken into account. An alternative being considered is not to tunnel in a straight line but to bend the Main Linac into an arc so as to follow an equipotential. We begin here an examination of the effects that this would have on vertical dispersion, with its attendant consequences on synchrotron radiation and emittance growth. Two scenarios are studied: (a) gently bending the beam ``continuously'' to follow an equipotential surface, and (b) introducing sharper bends at a few sites in the linac so as to reduce the maximum sagitta produced. In both cases, and throughout this paper, we will adopt a minimalist approach, always making the smallest possible changes to the already existing NLC design. We are striving here only for some order of magnitude calculations, not a serious design study.

Fermilab FERMILAB-FN-690 May 2000

Estimates of dispersive effects in a bent NLC Main Linac

Leo Michelotti and Michael Syphers

April 10, 2000

Each arm of the NLC Main Linac is almost 11 km in length; including the final focus region, the total complex extends over 30 km. Were it to be constructed using straight-line tunneling, its sagitta relative to a gravitational equipotential surface would be about 18 meters. While that seems like a small number, its impact on pumping requirements is significant. Further, if the tunnel is dug using "cut-and-fill" methods, the increased cost of moving the extra dirt must also be taken into account.

An alternative being considered is not to tunnel in a straight line but to bend the Main Linac into an arc so as to follow an equipotential. We begin here an examination of the effects that this would have on vertical dispersion, with its attendant consequences on synchrotron radiation and emittance growth. Two scenarios are studied: (a) gently bending the beam "continuously" to follow an equipotential surface, and (b) introducing sharper bends at a few sites in the linac so as to reduce the maximum sagitta produced. In both cases, and throughout this paper, we will adopt a minimalist approach, always making the smallest possible changes to the already existing NLC design. We are striving here only for some order of magnitude calculations, not a serious design study.

1 Continual gentle bends

In our first scenario, the Main Linac remains as close as possible to an equipotential surface. Minimalism suggests that we try bending the beam by vertically translating already existing NLC quadrupoles, without introducing new elements or additional magnetic fields. We thus propose that steering be accomplished by precisely aligning all the quads "level" along the equipotential and then raising the vertically defocusing (D) quadrupoles to steer the beam through the centers of the vertically focusing (F) quads.[1] Bending at the D quad locations will minimize the generated dispersion.

To estimate the order of magnitude of dispersion produced by such an arrangement, we calculate (a) assuming a periodic sequence of magnets while (b) neglecting the effects of acceleration [6] and (c) keeping only leading terms in the bend angle.[2] Our

[1] The usual convention is for "F" ("D") to indicate a horizontally focusing (defocusing) quadrupole. We do the opposite here, because we are considering dynamics only in the vertical plane.

[2] Literally, this would require that the bend angle be some integer fraction of 2π, a restriction that we will ignore.

results will be reasonably correct provided that upstream injection into the Main Linac is redesigned to match the new arrangement.

Figure 1 shows the physical layout of quadrupoles and identifies the geometric parameters. All length measurements are referred to a straight line passing through the center of two successive focussing quads: L is the "half-cell" length, that is, the (projected) distance between neighboring D and F quadrupoles; d, the vertical displacement of the D quad; y_o, the offset of the beam as it passes through the quad; y_{sag}, the sagitta of the equipotential at the quad's location; and finally, θ is the bend angle produced by the displaced D quad. A few geometric relations will be useful later; in what follows, R is the radius of the Earth.

$$\begin{aligned} L &= R\sin(\theta/2) \\ &\approx R\theta/2 \qquad (1) \\ y_o &= L\tan(\theta/2) \\ &\approx L\theta/2 \\ &\approx L^2/R \qquad (2) \\ y_{sag} &= R(\,1-\cos(\theta/2)\,) \\ &\approx R\theta^2/8 \\ &\approx L^2/2R \qquad (3) \end{aligned}$$

Of course, Eq.(1) was employed to eliminate θ from Eqs. (2) and (3). We note in passing that $y_o = 2y_{sag}$.

The offset, $y = d - y_o$, of the beam relative to the center of the D quad is obtained by exploiting symmetry: the quad converts $y' = -\tan(\theta/2) \approx -\theta/2$ to $y' = \tan(\theta/2) \approx \theta/2$. In the thin quadrupole approximation we therefore have,

$$\Delta y' \approx \theta = \frac{y}{f} = \frac{d-y_o}{f}\ , \qquad (4)$$

where f is the focal length of the quadrupole.[3]

While d represents the offset of the D quad relative to the center line, it is more practical to write its offset relative to the equipotential. This can be done by combining Eqs. (2), (3), and (4).

$$d - y_{sag} = (d-y_o) + (y_o - y_{sag}) = f\,\theta + L^2/2R$$

For convenience, we will eliminate f in favor of the phase advance per cell, μ, using the relation for a thin lens FODO cell, obtained by "circular reasoning" [6],

$$\sin(\mu/2) = \frac{L}{2f}\ , \qquad (5)$$

[3] In the thin lens approximation, $\Delta y'$ is approximately independent of the initial y' if the angles are sufficiently small. More correctly, this independence applies to the change in transverse momentum. For a discussion, see reference [5].

while simultaneously using Eq.(1) to eliminate θ.

$$\begin{aligned} d - y_{\rm sag} &= \left(\frac{L}{2\sin(\mu/2)}\right)\left(\frac{2L}{R}\right) + \frac{L^2}{2R} \\ &= \frac{L^2}{R}\left(\frac{1}{2} + \frac{1}{\sin(\mu/2)}\right) \end{aligned} \tag{6}$$

To make a numerical estimate of this offset at the high energy end of the linac, we take $L \approx 19\,\mathrm{m}$, $\mu \approx \pi/2$, and $R \approx 6400\,\mathrm{km}$. Eq.(6) then yields $d - y_{\rm sag} \approx 108\,\mu\mathrm{m}$.

Dispersion.

The dispersion can be estimated easily using two observations: (1) in passing through a thin bending magnet, the slope of the dispersion function, D', changes by an amount approximately equal to the bend angle; (2) by symmetry, the dispersion attains its maximum (minimum) value at the center of the focussing (defocussing) quadrupole. Imagine replacing the offset thin (defocussing) quadrupole with a sandwich of four elements, all on-axis: a thin quadrupole, two thin dipoles, and another thin quadrupole, each element at half strength. The focussing quadrupole is replaced by two thin quadrupoles of half strength, with no intermediate dipoles. In passing from the center of the defocussing sandwich through one of the thin dipoles, the dispersion state vector changes

$$\text{from} \quad \begin{pmatrix} D_{\rm min} \\ 0 \end{pmatrix} \quad \text{to} \quad \begin{pmatrix} D_{\rm min} \\ \theta/2 \end{pmatrix} .$$

We obtain the following equation by following this state vector through the remaining elements to the middle of the focussing quad.

$$\begin{aligned} \begin{pmatrix} D_{\rm max} \\ 0 \end{pmatrix} &= \begin{pmatrix} 1 & 0 \\ -1/2f & 1 \end{pmatrix}\begin{pmatrix} 1 & L \\ 0 & 1 \end{pmatrix}\begin{pmatrix} 1 & 0 \\ 1/2f & 1 \end{pmatrix}\begin{pmatrix} D_{\rm min} \\ \theta/2 \end{pmatrix} \\ &= \begin{pmatrix} 1+L/2f & L \\ -L/(2f)^2 & 1-L/2f \end{pmatrix}\begin{pmatrix} D_{\rm min} \\ \theta/2 \end{pmatrix} \end{aligned}$$

The bottom component provides the value of $D_{\rm min}$; this, in combination with the top

component, then gives us $D_{\max}$.

$$\begin{aligned} 0 &= -D_{\min}\frac{L}{(2f)^2} + \frac{\theta}{2}\left(1-\frac{L}{2f}\right) \\ \Rightarrow D_{\min} &= \frac{2f}{L}\left(1-\frac{L}{2f}\right)\cdot f\theta \\ &= \frac{f\theta}{\sin(\mu/2)}\,(1-\sin(\mu/2)\,) \\ D_{\max} &= \left(1+\frac{L}{2f}\right)D_{\min} + L\frac{\theta}{2} \\ &= (1+\sin(\mu/2)\,)D_{\min} + \sin(\mu/2)\,f\theta \\ &= \frac{\cos^2(\mu/2)}{\sin(\mu/2)}\,f\theta + \sin(\mu/2)\,f\theta \\ &= \frac{f\theta}{\sin(\mu/2)} \end{aligned}$$

Notice that $D_{\max} - D_{\min} = f\theta = y$. Our final step is to substitute for $f\theta$ using Eqs. (1) and (5).

$$\begin{aligned} D_{\min} &= \frac{L^2}{R\sin^2(\mu/2)}\,(1-\sin(\mu/2)\,) \\ D_{\max} &= \frac{L^2}{R\sin^2(\mu/2)} \end{aligned}$$

Using the same parameters as before, this provides the numerical estimate, at the high energy end of the linac,

$$D_{\min} = 0.032\,\text{mm}, \quad D_{\max} = 0.11\,\text{mm}.$$

If we take a large $\Delta p/p \approx \Delta E/E = 0.02$, because of BNS damping, and assume that the "invariant emittance" $\gamma\varepsilon_y/\pi \approx 100\,\text{nm}$ and $\beta_y \approx 40$ m at a point where the electron's energy is $E = 100$ GeV, then

$$D_{\max}\cdot\frac{\Delta p}{p} = 2.2\,\mu\text{m} \quad \text{compared to} \quad \sigma_y = \sqrt{\beta_y\varepsilon_y/\pi} = 4.6\,\mu\text{m}\,. \tag{7}$$

Synchrotron radiation.

Vertical bending will produce synchrotron radiation, which, in its turn, will add to the vertical emittance of the beam. At high energy, the total energy radiated by one electron is given by the expression,[4]

$$U = \int (cdt)\frac{1}{6\pi\varepsilon_o}\left(\frac{e}{\rho}\right)^2\gamma^4\,,$$

[4] See, for example, Equations 8.6 and 8.10 of Edwards and Syphers. [3]

where, ρ is the bend radius, γ is the relativistic $1/\sqrt{1-(v/c)^2}$, and the other variables need no introduction.[5] If we substitute

$$\begin{aligned}\int (cdt) &\approx \ell, \quad \text{the length of the quad,}\\ \gamma &= E/mc^2,\\ \rho\theta &\approx \ell, \quad \text{and use}\\ e^2 &= 4\pi\varepsilon_o mc^2 r_e\end{aligned}$$

then we obtain the result,

$$\begin{aligned}U &\approx \left(\frac{2}{3}\frac{r_e}{(mc^2)^3}\right) E^4 \ell \langle 1/\rho^2\rangle\\ &\approx (1.41\times 10^{-5}\,\mathrm{m\,GeV^{-3}})\cdot E^4\theta^2/\ell\,. \qquad (8)\end{aligned}$$

Using the same parameters as before, $\theta \approx 5.6\,\mu$rad; at the high energy end of the linac, $E \approx 500$ GeV, and $\ell \approx 1$ m; our estimate of the total radiated energy (per electron per bend) is about 28 keV. Put another way, the ratio, $U/E \approx 6\times 10^{-8}$.

Emittance growth.

It is inconceivable that such a small fractional change in beam energy could seriously damage the emittance, but we will estimate its effect anyway. The additional invariant emittance due to synchrotron radiation is approximated as[6]

$$\Delta(\gamma\varepsilon_y/\pi) = \Delta(\gamma\sigma_y^2/\beta_y) \approx \frac{1}{2mc^2} N\,(D_{\max}^2/\beta_y)\,\frac{\sigma_w^2}{E}, \quad \text{where} \qquad (9)$$

$$\begin{aligned}N &= U/\overline{w}\,, \quad \text{the expected number of photons emitted per electron,}\\ \overline{w} &= \frac{4}{5\sqrt{3}}\gamma^3\hbar\frac{d\theta}{dt}\\ &\approx \frac{4}{5\sqrt{3}}\left(\frac{E}{mc^2}\right)^3 \hbar c(\theta/\ell), \quad \text{average energy per photon,}\\ \sigma_w^2 &= 34\frac{3}{8}\overline{w}^2, \quad \text{variance of photon energies.}\end{aligned}$$

This expresses the fact that a variance in energies of the radiated photons feeds into the energy spread in the beam, which we convert, via the local dispersion, into an increased invariant emittance. Except for noting that $\Delta(\gamma\varepsilon_y/\pi)$ scales as E^6/ρ^3, we will forego the pleasure of simplifying these equations, preferring a numerical calculation. Plugging in the same numbers as before, estimating $\beta_y \approx 60$ m, and using our previous estimates for U and $D_{\max}$, we obtain, $\Delta(\gamma\varepsilon_y/\pi) \approx 1.8\times 10^{-7}$ nm – as expected, a very small number.

[5] Throughout the following discussion, we will avoid confusion of relativistic symbols with their equivalent lattice function symbols by using β_y, α_y, and γ_y for the latter. This will have the additional advantage of constantly reminding us that they refer to the vertical plane.

[6] The equations we use here are explained in Section 8.3 of Edwards and Syphers. [3] In writing it this way we are using the "fact" that both D and and β_y achieve their maximum value at the same point, so that $\gamma_y D_{\max}^2 = D_{\max}^2/\beta_y$, since $\alpha_y = 0$ at that point.

2 Localized sharp bends

Although the 2 μm offset predicted by Eq.(7) is not catastrophic, neither is it completely negligible. We will now consider eliminating it by employing the second scenario: constructing a Main Linac that is laser straight except for highly localized bends at a few, widely separated locations. These bend sites then allow us to follow the equipotential in a coarser, piece-wise fashion. If we think of bending every kilometer, or so, then the bend angle should be about 160 μrad. We'll take this as the "canonical" value for calculations in this section.

We will proceed again in a minimalist way. However, this time we cannot bend the beam by displacing quadrupoles; Eq.(4) indicates that the beam would have to pass through the quad about 5 or 6 cm off axis. As alternatives, (a) new bend sections could be inserted into the lattice, matching linear optics with Main Linac cells upstream and downstream, (b) new dipoles could be inserted into already existing drift spaces, or (c) dipole fields could be introduced into a few already existing quadrupoles, changing them into combined function elements. The last strategy represents a smaller modification of existing lattice hardware and optics, so we will adopt it here. Other possibilities could be considered at a later date.

Dispersion.

For a reason soon to be made apparent, the total bend angle is distributed across four neighboring (combined function) dipoles, as shown in Figure (2a). (For the time being, ignore Figure (2b).) The dispersion wave that this would launch is illustrated in Figure 3. For this calculation, horizontal dipole fields have been added to four quadrupoles — QQ0503, QQ0504, QQ0505, and QQ0506, near the beginning of the Main Linac's Line 2 — so that each element bends the beam through 40 μrad. To keep matters simple, it is assumed that sector bends are used so that (a) the "fiducial" or "reference" orbit passes through the zero of the quadrupole component and (b) we may ignore edge focussing associated with a rectangular magnet. The curves plotted in Figure 3 illustrate two definitions of "dispersion," which is essentially a differential of an orbit with respect to fractional momentum, $\Delta p/p$: the calculation of the solid curve used $\Delta p/p$ at the entrance to the Main Linac, while local $\Delta p/p$ was used to produce the dashed curve. Physics and orbit differentials are the same in both cases; the differences are only a matter of presentation. The first definition makes it easier to compare orbits at different locations in the linac. However, emittance growth from synchrotron radiation depends on the *local* definition, so we will use it in all subsequent calculations, and prefix a "local" label as a reminder.

Figure 4 shows local dispersion waves launched at ten locations separated by about 1 km; initial wave amplitudes are about 4 mm at the high energy end of the linac. Each one has been truncated after a few oscillations, and the individual dispersions have not been summed. The dipole fields required to bend the beam through 40 μrad at each location – as was sketched in Figure (2a) – can be found in the second column of Table 1. Field values grow from ≈ 160 Gauss to ≈ 650 Gauss because the beam energy increases between the combined function elements.

Achromats.

It is difficult for one accustomed to dispersions on the order of meters to think that a 4 mm dispersion wave is a matter of concern. However, putting this number back into Eq.(7), we see that

$$D_{\max} \cdot \frac{\Delta p}{p} = 80\,\mu\text{m} \quad \text{compared to} \quad \sigma_y = \sqrt{\beta_{\max}\varepsilon_y/\pi} = 4.6\,\mu\text{m}$$

In absolute terms, 80 μm seems a small number, but, as it is more than an order of magnitude greater than the beam width expected from transverse emittance, we will consider removing the dispersion by bending the beam with a "partial" achromat.

Again, we adopt a minimalist approach, making the fewest changes to the already existing design. Achromats in accelerator physics have been studied from several points of view. [1, 2, 4, 7, 8, 9, 10] Typically, symmetries or special arrangements of elements in the design result in cancellations, resulting in a beamline that is "transparent" in all six phase space variables. Although there are some exceptions [7], most people seem to define "achromat" using this condition, according to which the transfer map through an "achromat" is equivalent, at some order, to the identity. We employ a much less restrictive criterion; our "achromat" will impose only the condition that two particles with differing momenta end up on the same orbit after the bend. Our strategy is akin to that of an 18^{th} century optician designing a simple focussing achromat, as shown in Figure 5. A focussing lens is replaced by a sandwich of defocussing and focussing lenses, arranged so that light of two colors at opposite ends of the spectrum have the same focal point, the idea being that intermediate colors would then be not far off. This is accomplished by bending rays in the "wrong" direction and compensating with the second lens. Figure (2b) illustrates how we must analogously distort the fiducial orbit by underbending with one magnet and compensating with another. Four magnets are necessary to preserve both the bend angle and the overall bend center in going from Figure (2a) to Figure (2b) while simultaneously getting particles with different momenta to finally end up on the same orbit.

The third column in Table 1, the one labelled "Adjusted Field," contains the dipole fields required to accomplish this distorted, "partial achromatic" orbit, maintaining the 160 μrad bend angle and the overall bend center while zeroing the residual dispersion. At each location, the maximum fields are an order of magnitude larger than the original ones in Column 2. Because we have chosen not to reposition the magnets, their quadrupole components also contribute to the bend; for completeness, the table's last column lists the "effective" dipole field on the (off-axis) fiducial orbit produced by the quadrupole component. (Values smaller than 10 Gauss have been suppressed.) If the momentum were the same at every bend site, – which it is not; the accelerating cavities are not turned off – the total integrated dipole field in the second column would be the same as that from the last two columns. Even so, the relative change in momentum is small, and the sums are approximately identical. For example, at the first site, beginning with QQ0503, the summed dipole field from column 2 is an ominous 666 Gauss, while that from columns 3 and 4 is 674 Gauss.

Notice, by the way, that Figure (2b) did not portray the sense of the bends correctly. Both positive and negative fields appear in the actual solutions. It is necessary to "bend

in the wrong direction" in order to accomplish the achromat's objective.

The results at the lowest energy location are shown in Figure 6. The dashed line follows the residual dispersion, now completely contained within the ≈ 40 m long bending region, with maximum amplitude of about 0.6 mm. All values are expressed relative to the curved reference orbit shown in Figure (2a). The maximum orbit distortion of 1 mm is too large an offset from the central (curved) axis of the local bending magnets. They would have to be displaced so as to follow the new orbit. A few iterations of these manipulations should then converge on an acceptable design. However, the final orbit and its local residual dispersion should not be much different from what we have calculated here. For now, we simply display these results as indicating the order of magnitude of the effects.

The orbit distortions at all ten locations — three in Line 2, seven in Line 3 — are plotted in Figure 7; the corresponding dispersions are shown in Figure 8. A residual dispersion of 1 mm remains in the neighborhood of the bends. Again assuming that $\Delta p/p \approx 0.02$, we have

$$D_{\max} \cdot \frac{\Delta p}{p} = 20\,\mu\text{m} \quad \text{compared to} \quad \sigma_y = \sqrt{\beta_{\max}\varepsilon_y/\pi} = 4.6\,\mu\text{m}$$

This is a large increase, but *it exists only near the bend sites.* Away from these sites, the dispersion is (essentially) zero, and its contribution to emittance is negligible.

We note in passing that an advantage of this calculation is that one can envision making it operational. Nonetheless, the model that was used possesses a number of unrealistic features:

- No displacements were made to any elements. The resultant beam offsets in the quads and cavities would have to be zeroed by displacing these elements and iterating to find new solutions.
- Both dipole and quadrupole components contribute to the bend angles, making control more difficult. Repositioning the elements so as to return the design orbit to their central axis would solve this problem as well.
- RF cavities were left turned on. Energy increased throughout the bend, and, because of transverse deceleration, the cavity itself contributed to the solution. This can be corrected either (a) by realigning the cavities along the new design orbit or (b) removing the cavities entirely from the bending regions and compensating elsewhere in the lines. The former alternative could be difficult to achieve in practice; the second would have a very small (negligible) effect on the transverse lattice functions, assuming that the quad strengths are also modified in order to match correctly into the next cell.

These deficiencies are accidental, not essential, features of our analysis. All of them can be corrected in more refined calculations, and the required changes should not significantly alter the final results.

Synchrotron radiation and emittance growth.

Finally, we estimate the synchrotron radiation and emittance growth incurred by our second scenario, once again using Eqs.(8) and (9). Values of the variables entering into these calculations have been tabulated in Table 2 for easy reference; the lengths, ℓ, are 43 cm for the three sets of quads in Line 2 and 98 cm for the seven sets of quads in Line 3. To ease the clutter a little, values smaller than 10^{-3}, in their respective units, have been suppressed.

The values of $\Delta(\gamma\varepsilon_y/\pi)$ at all bend locations are plotted in Figure 9. Each site contains one dominant, very sharp bend. Its effect is most apparent near the high energy end of the linac, where the E^6 dependence becomes overwhelming. Even so, the additional ≈ 1 nm in invariant emittance is less than 1% of the 140 nm vertical emittance expected within the interaction region.

Notice that although the synchrotron radiation is rather high at the end of the linac, the ratio

$$U/E = 49 \text{ MeV}/473 \text{ GeV} \approx 10^{-4} \ .$$

is still a small number.

Coherent synchrotron radiation.

So far, we have considered incoherent synchrotron radiation only, not unreasonably, since the average wavelength of emitted photons is about 5×10^{-4} angstroms. The spectrum is "almost zero" out at wavelengths comparable to the bunch size of approximately 150 μm. Nonetheless, with almost 10^{11} electrons in a bunch, and with the smallest radius of curvature recorded in Table 2 being only a few kilometers long, some attention should be given to the possibility of coherent synchrotron radiation (CSR) from the bunch as a whole.

The CSR spectrum has support within the wavelength range,

$$\sigma_z < \lambda < 2a\sqrt{a/\rho} \ ,$$

where σ_z is the longitudinal bunch length, a is a transverse dimension (e.g., radius) of the beam pipe, and ρ is the radius of curvature. These inequalities are approximate: the one on the left expresses the fact that λ must be larger than internal structure within the bunch for the radiation to build coherently; the one on the right is a cutoff for propagation in the presence of walls and the source bunch. [11, 12, 13] From these, we see that no CSR is possible unless

$$(\sigma_z\sqrt{\rho}/2)^{2/3} < a$$

Plugging in $\sigma_z \approx 150\,\mu$m and $\rho \approx 3$ km results in the requirement, $a \geq 26$ mm, for CSR to occur. Current design has $a \approx 7$ mm, so CSR is forbidden, even at the high energy end of the linac, because of "shielding" from the walls of the beam pipe. However, the margin of safety is not comfortably large. It may be necessary to reexamine this issue.

3 Conclusions

We have estimated the dispersive effects produced by bending a beam in the NLC Main Linac using two scenarios. In the first we assumed a series of small bends continually distributed along the linac. Approximating the resulting dispersion as what would be obtained in a periodic lattice, we found the numbers to be small enough to be negligible. In the second we established a small number of sharper bends at discrete locations in the linac. In such a case, by choosing the bend fields appropriately, we localize the dispersion to the region of the bend. While the resultant synchrotron radiation is large near the high energy end of the linac, the calculated emittance growth remains comfortably small. Coherent synchrotron radiation is barely suppressed by the beam pipe.

Neither of the strategies was developed to the point of being a legitimate design. We have pointed out ways in which they can be refined and extended if there is a desire to continue pursuing this subject.

Acknowledgements

We are grateful to Courtlandt Bohn for carefully reading our manuscript and suggesting the possible importance of coherent synchrotron radiation.

References

[1] K. L. Brown. A second order magnetic optical achromat. *IEEE Trans. Nucl. Sci.*, 26:3490, 1979. (Preprint: SLAC-PUB-2257. Feb, 1979).

[2] David C. Carey. Why a second order magnetic optical achromat works. *Nucl. Instr. Meth.*, 189:365, 1981. (FERMILAB-Pub-79/61-EXP 2042.000. Feb, 1980.).

[3] D. A. Edwards and M. J. Syphers. *An Introduction to the Physics of High Energy Accelerators*. John Wiley & Sons, New York, 1993.

[4] S. A. Kheifets, T. H. Fieguth, and R. D. Ruth. Canonical description of a second-order achromat. SLAC-PUB-4569. (Presented at the Second ICFA Advanced Beam Dynamics Workshop. Lugano, Switzerland. April 11-16, 1988.), March 1988.

[5] Leo Michelotti. Passage through a transverse magnetic slab. FERMILAB-TM-2059, October 1998.

[6] Leo Michelotti. A two-parameter accelerating FODO cell. FERMILAB-FN-688, January 2000.

[7] D. Raparia, J. G. Alessi, Y. Y. Lee, and W. T. Weng. Achromat with linear space charge for bunched beams. Presented at the XIX International Linear Accelerator Conference. Chicago, IL., 1998.

[8] L. C. Teng. Symmetric achromatic beam transport system. Fermilab FN-128, April 1968.

[9] W. Wan and M. Berz. Design of a fifth-order achromat. *Nucl. Instrum. Meth.*, A423:1, 1999.

[10] Chunxi Wang and Alex Chao. Analytic second- and third-order achromat designs. SLAC-PUB-95-6794. (Talk given at 16th IEEE Particle Accelerator Conference (PAC 95) and International Conference on High Energy Accelerators (IUPAP), Dallas, Texas, 1-5 May 1995), July 1995.

[11] R. L. Warnock and P. Morton. *Particle Accelerators*, 25:113, 1990.

[12] Robert Lee Warnock. Shielded coherent synchrotron radiation and its effect on very short bunches. Presented at 4th Advanced ICFA Beam Dynamics Workshop on Collective Effects in Short Bunches, Tsukuba, Japan. September 24-29, 1990., September 1990.

[13] Robert Lee Warnock. Shielded coherent synchrotron radiation and its possible effect in the next linear collider. SLAC-PUB-5523. Presented at IEEE PArticle Accelerator Conf., San Francisco, CA. May 6-9, 1991, May 1991.

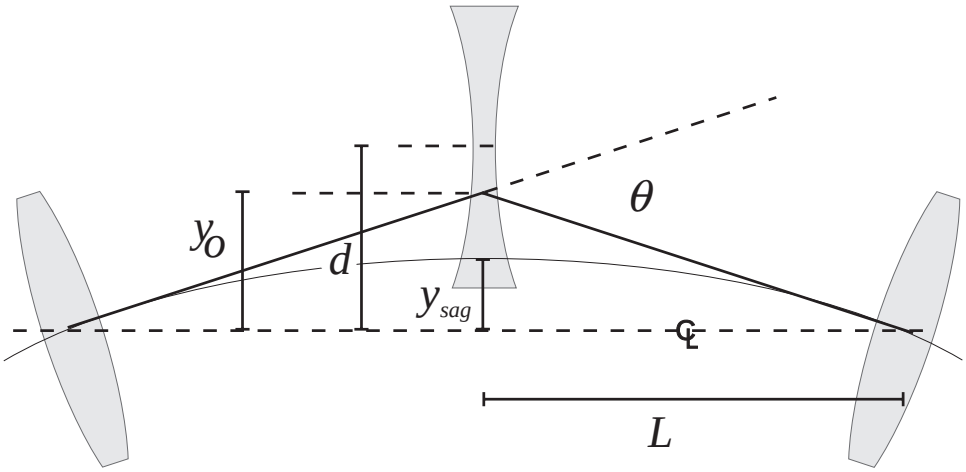

Figure 1: Description of parameters for describing the CR thin quad calculations.

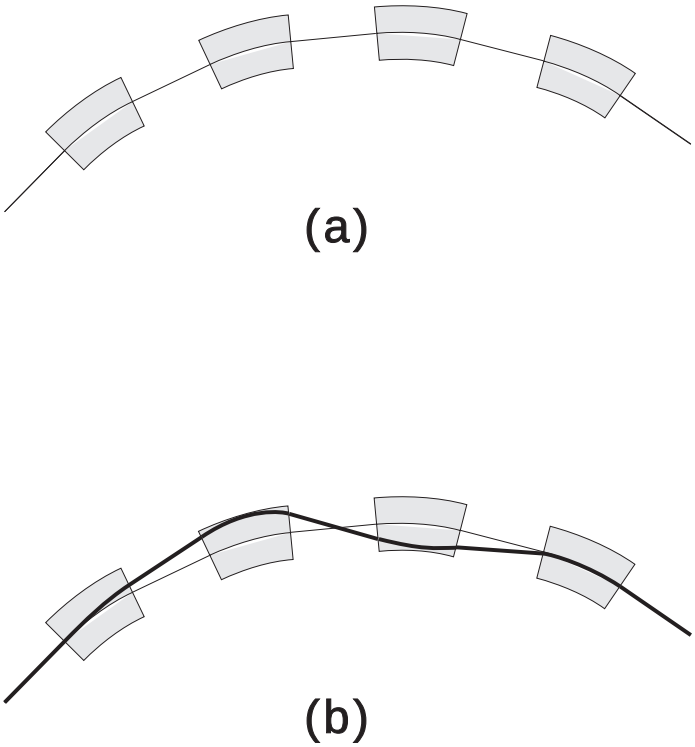

Figure 2: (a) Gently bending a beam using four dipoles. (b) Achromat strategy sketched out: four dipoles.

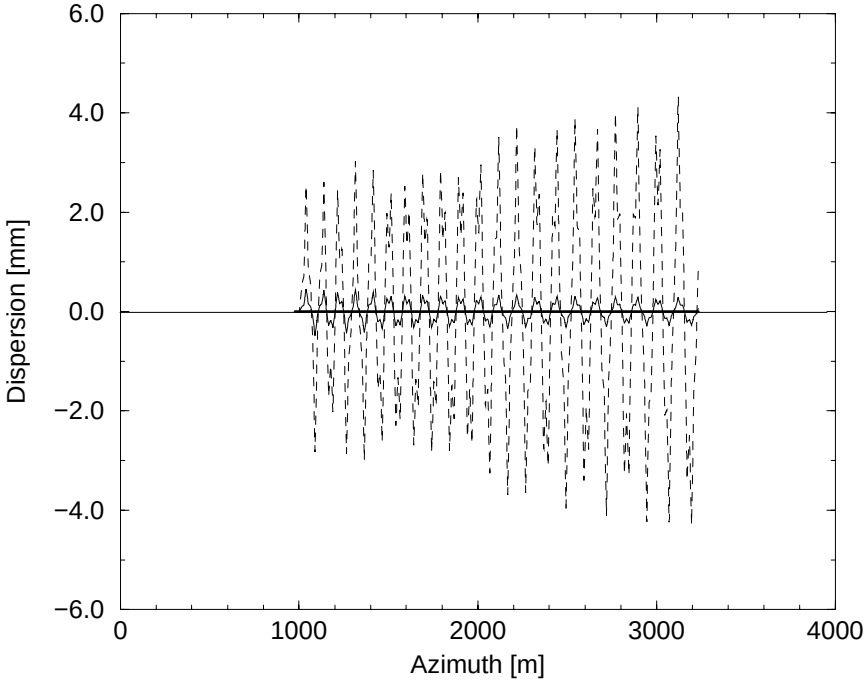

Figure 3: Dispersion launched by a 160 μrad bend.

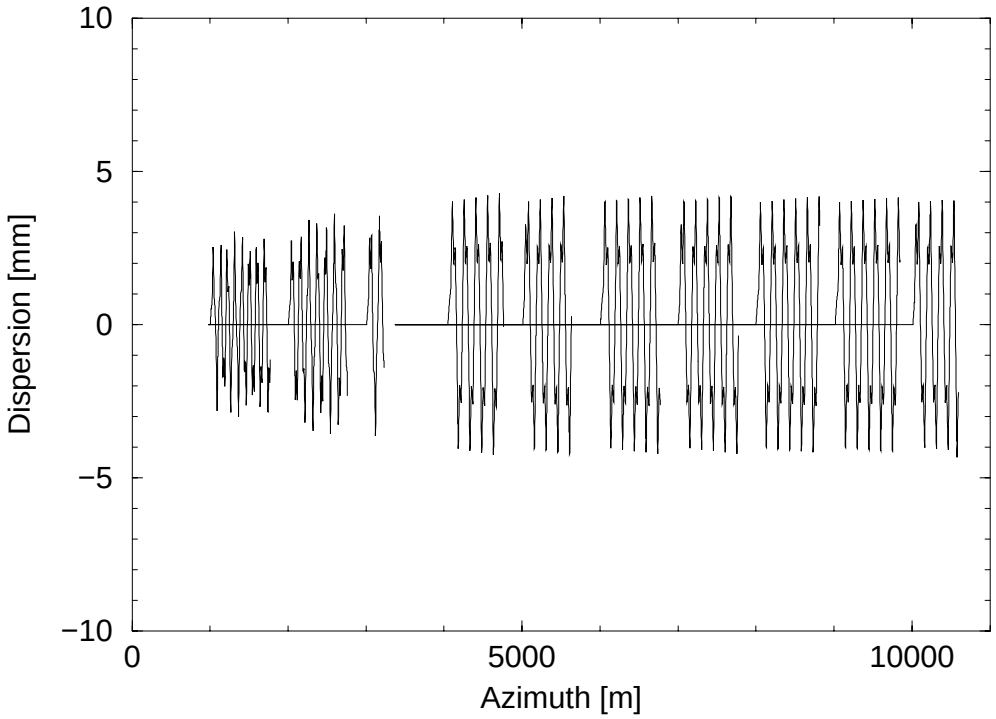

Figure 4: Local dispersion waves launched at ten locations.

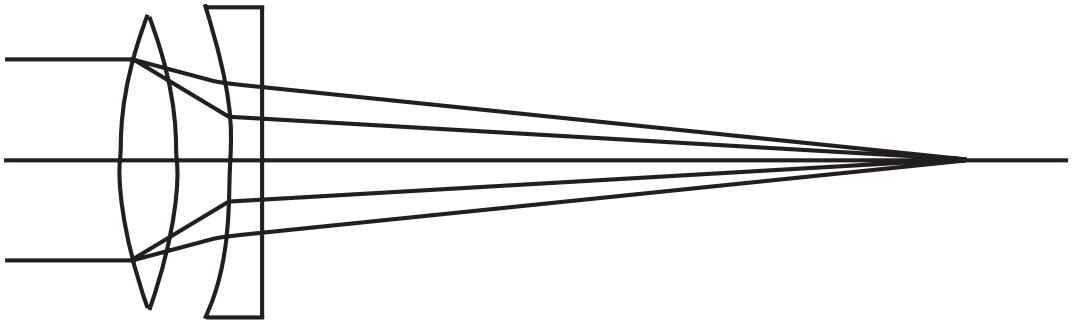

Figure 5: Illustration of achromat lens, designed to focus light of two wavelengths to the same point.

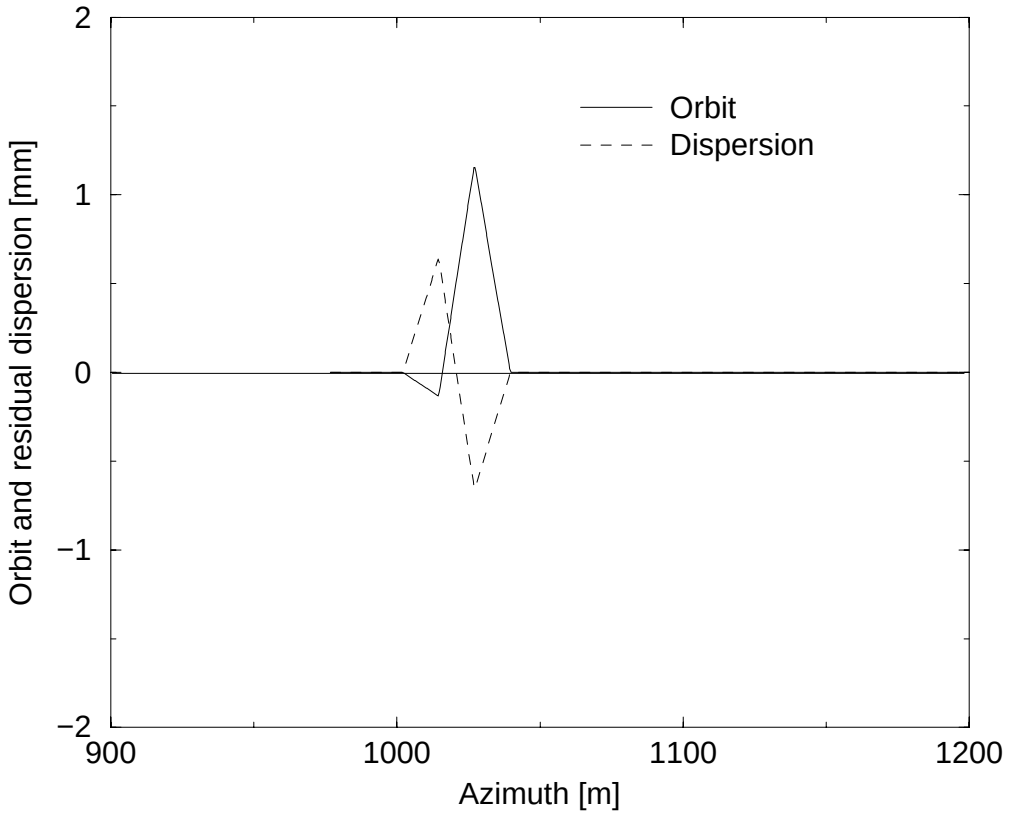

Figure 6: Orbit deviation required to zero the residual dispersion.

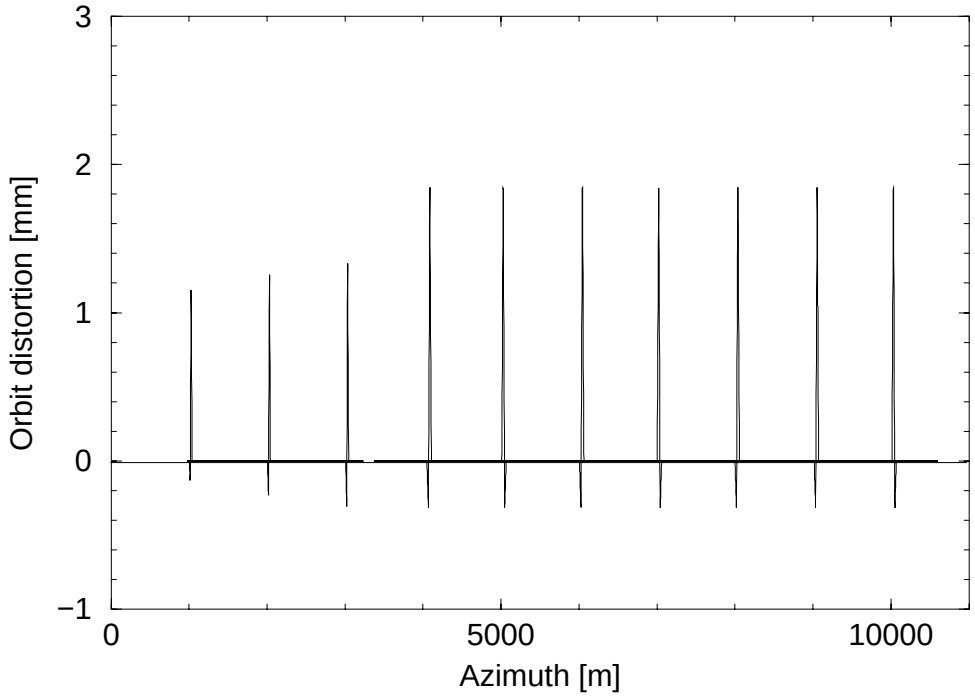

Figure 7: Orbit deviations required by the partial achromats at all ten locations.

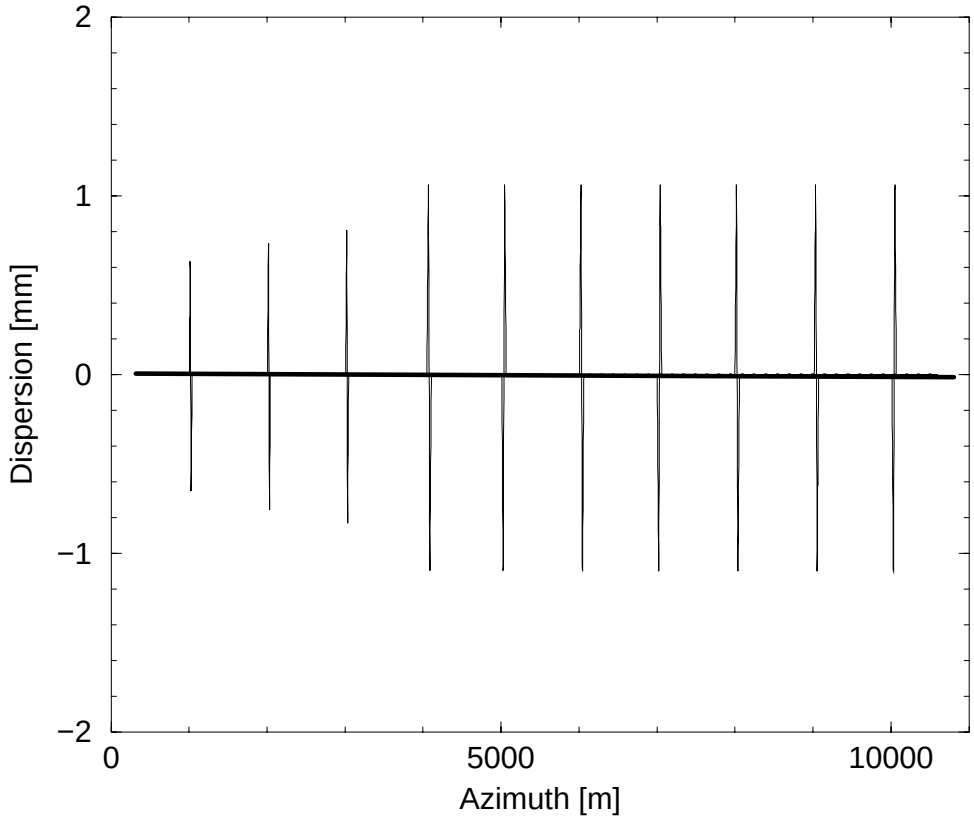

Figure 8: Corresponding residual dispersion.

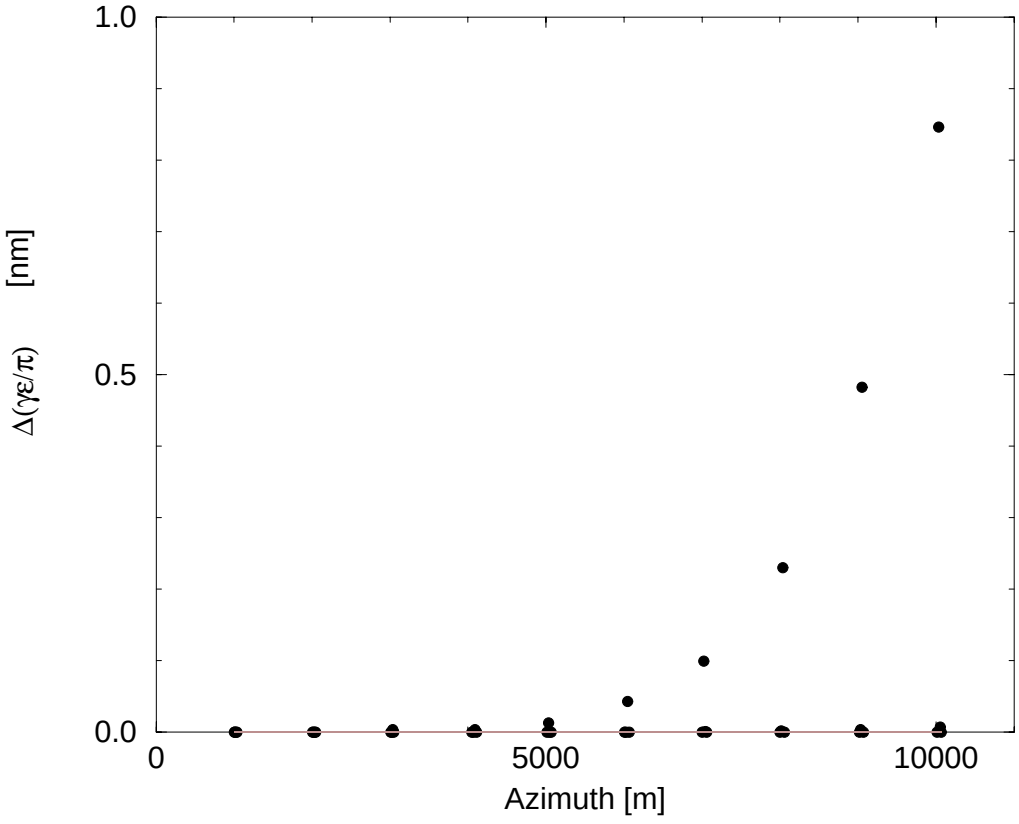

Figure 9: Emittance growth due to synchrotron radiation in sharp bends.

Magnet	Original Field [Tesla]	Adjusted Field [Tesla]	Quad Field [Tesla]
QQ0503:	0.0164	0.0207	
QQ0504:	0.0166	-0.0247	-0.00586
QQ0505:	0.0167	0.159	-0.0597
QQ0506:	0.0169	-0.0228	
QQ0911:	0.0307	0.0452	
QQ0912:	0.0309	-0.0582	-0.0178
QQ0913:	0.0311	0.309	-0.104
QQ0914:	0.0313	-0.0490	
QQ1401:	0.0452	0.0733	
QQ1402:	0.0453	-0.100	-0.0321
QQ1403:	0.0455	0.468	-0.147
QQ1404:	0.0457	-0.0785	
QQ1801:	0.0260	0.0371	
QQ1802:	0.0261	-0.0474	-0.0131
QQ1803:	0.0263	0.260	-0.0895
QQ1804:	0.0264	-0.0408	
QQ2204:	0.0322	-0.0499	0.00303
QQ2205:	0.0323	0.319	-0.109
QQ2206:	0.0324	-0.0584	-0.0196
QQ2207:	0.0326	0.0465	
QQ2609:	0.0386	0.0550	
QQ2610:	0.0387	-0.0703	-0.0195
QQ2611:	0.0389	0.385	-0.132
QQ2612:	0.0390	-0.0604	
QQ3102:	0.0450	-0.0699	0.00424
QQ3103:	0.0452	0.446	-0.152
QQ3104:	0.0453	-0.0816	-0.0273
QQ3105:	0.0454	0.0648	
QQ3507:	0.0515	0.0734	
QQ3508:	0.0516	-0.0934	-0.0260
QQ3509:	0.0517	0.511	-0.175
QQ3510:	0.0518	-0.0803	
QQ4001:	0.0580	0.0827	
QQ4002:	0.0581	-0.105	-0.0293
QQ4003:	0.0582	0.576	-0.198
QQ4004:	0.0584	-0.0904	
QQ4406:	0.0644	-0.0999	0.00607
QQ4407:	0.0645	0.638	-0.218
QQ4408:	0.0647	-0.116	-0.0390
QQ4409:	0.0648	0.0925	

Table 1: Magnetic fields producing the bends.

Magnet	E [GeV]	γ	ρ [km]	σ_w [MeV]	U [MeV]
		N	β_y [m]	D [mm]	$\Delta(\gamma\varepsilon_y/\pi)$ [nm]
QQ0503:	53.79	105268	8.617	0.0256	
		0.0564	5.66	0.0111	
QQ0504:	54.38	106426	-5.829	0.0391	0.00159
		0.0843	44.6	0.622	
QQ0505:	54.98	107584	1.834	0.128	0.0168
		0.271	5.58	-0.652	
QQ0506:	55.57	108742	-8.302	0.0293	
		0.0605	44.8		
QQ0911:	101.1	197915	7.421	0.197	0.0117
		0.123	8.2	0.013	
QQ0912:	101.7	199073	-4.399	0.339	0.0341
		0.209	41	0.72	
QQ0913:	102.3	200231	1.662	0.913	0.245
		0.556	8.09	-0.756	
QQ0914:	102.9	201389	-7.145	0.216	0.0136
		0.13	40.8		
QQ1401:	148.5	290562	6.724	0.689	0.0663
		0.199	10	0.0143	
QQ1402:	149.1	291720	-3.719	1.26	0.22
		0.362	40.4	0.794	
QQ1403:	149.7	292878	1.554	3.05	1.28
		0.87	9.89	-0.831	0.00371
QQ1404:	150.3	294036	-6.492	0.74	0.0746
		0.209	40.3		
QQ1801:	191.1	373945	17.08	0.578	0.0629
		0.226	11.6	0.0282	
QQ1802:	192	375682	-10.35	0.968	0.175
		0.374	62.5	1.03	
QQ1803:	192.9	377419	3.762	2.7	1.35
		1.03	11.3	-1.1	0.00408
QQ1804:	193.8	379156	-16.3	0.632	0.073
		0.24	60.3		
QQ2204:	236.4	462538	-16.27	1.15	0.162
		0.293	60.3	-0.0298	
QQ2205:	237.2	464276	3.766	5.02	3.08
		1.27	11.6	-1.07	0.013
QQ2206:	238.1	466013	-10.38	1.84	0.411
		0.463	62.5	1.06	
QQ2207:	239	467750	17.03	1.14	0.155
		0.283	11.3		

Table 2: Quantities entering the emittance growth calculation.

Magnet	E [GeV]	γ	ρ [km]	σ_w [MeV]	U [MeV]
		N	β_y [m]	D [mm]	$\Delta(\gamma\varepsilon_y/\pi)$ [nm]
QQ2609:	283.4	554606	17.06	1.89	0.305
		0.335	11.6	0.0276	
QQ2610:	284.3	556344	-10.34	3.14	0.84
		0.554	62.5	1.03	
QQ2611:	285.2	558081	3.76	8.73	6.44
		1.53	11.3	-1.1	0.0428
QQ2612:	286.1	559818	-16.28	2.04	0.348
		0.354	60.3	-0.00219	
QQ3102:	330.5	646675	-16.26	3.14	0.621
		0.41	62.5	-0.0299	
QQ3103:	331.3	648412	3.764	13.7	11.7
		1.77	11.3	-1.07	0.0995
QQ3104:	332.2	650149	-10.36	5.01	1.56
		0.646	60.2	1.06	
QQ3105:	333.1	651886	17.03	3.07	0.584
		0.394	11.6		
QQ3507:	377.5	738743	17.06	4.46	0.961
		0.446	11.3	0.028	
QQ3508:	378.4	740480	-10.35	7.41	2.63
		0.737	60.2	1.03	0.00185
QQ3509:	379.3	742217	3.762	20.5	20.1
		2.03	11.6	-1.1	0.23
QQ3510:	380.2	743954	-16.28	4.78	1.08
		0.471	62.5		
QQ4001:	425.4	832548	17.06	6.39	1.55
		0.503	11.6	0.0281	
QQ4002:	426.3	834285	-10.35	10.6	4.24
		0.83	62.6	1.03	0.00364
QQ4003:	427.2	836022	3.762	29.3	32.4
		2.29	11.3	-1.1	0.482
QQ4004:	428.1	837759	-16.28	6.82	1.74
		0.53	60.2	0	0
QQ4406:	472.5	924616	-16.26	9.18	2.59
		0.586	62.6	-0.0299	
QQ4407:	473.4	926353	3.763	39.9	48.8
		2.54	11.3	-1.07	0.846
QQ4408:	474.3	928090	-10.36	14.6	6.49
		0.923	60.2	1.06	0.00756
QQ4409:	475.1	929827	17.03	8.92	2.42
		0.562	11.6		

Table 2: (cont.) Quantities entering the emittance growth calculation.